AMERICAN SOCIETY FOR MICROBIOLOGY | Journal of Virology®

PATHOGENESIS AND IMMUNITY

A Neonatal Murine Model of Coxsackievirus A6 Infection for Evaluation of Antiviral and Vaccine Efficacy

Zhenjie Zhang,[a] Zhaopeng Dong,[a,b] Qingjuan Wei,[c] Michael J. Carr,[d,e] Juan Li,[a] Shujun Ding,[f] Yigang Tong,[g] Dong Li,[b] Weifeng Shi[a]

Institute of Pathogen Biology, Taishan Medical College, Taian, Shandong, China[a]; School of Public Health, Taishan Medical College, Taian, Shandong, China[b]; Taian Maternal and Child Care Hospital, Taian, Shandong, China[c]; Global Station for Zoonosis Control, Global Institution for Collaborative Research and Education (GI-CoRE), Hokkaido University, Sapporo, Japan[d]; National Virus Reference Laboratory, University College Dublin, Dublin, Ireland[e]; Department of Viral Infectious Diseases Control and Prevention, Shandong Center for Disease Control and Prevention, Jinan, Shandong, China[f]; Beijing Institute of Microbiology and Epidemiology, Beijing, China[g]

ABSTRACT Hand, foot, and mouth disease (HFMD) is a global health concern. Family *Picornaviridae* members, particularly enterovirus A71 (EVA71) and coxsackievirus A16 (CVA16), are the primary etiological agents of HFMD; however, a third enterovirus A species, CVA6, has been recently associated with epidemic outbreaks. Study of the pathogenesis of CVA6 infection and development of antivirals and vaccines are hindered by a lack of appropriate animal models. We have developed and characterized a murine model of CVA6 infection that was employed to evaluate the antiviral activities of different drugs and the protective efficacies of CVA6-inactivated vaccines. Neonatal mice were susceptible to CVA6 infection via intramuscular inoculation, and the susceptibility of mice to CVA6 infection was age and dose dependent. Five-day-old mice infected with $10^{5.5}$ 50% tissue culture infective doses of the CVA6 WF057R strain consistently exhibited clinical signs, including reduced mobility, lower weight gain, and quadriplegia with significant pathology in the brain, hind limb skeletal muscles, and lungs of the infected mice in the moribund state. Immunohistochemical analysis and quantitative reverse transcription-PCR (qRT-PCR) analyses showed high viral loads (11 $\log_{10}$/mg) in skeletal muscle, and elevated levels of interleukin-6 (IL-6; >2,000 pg/ml) were associated with severe viral pneumonia and encephalitis. Ribavirin and gamma interferon administered prophylactically diminished CVA6-associated pathology *in vivo*, and treatment with IL-6 accelerated the death of neonatal mice. Both specific anti-CVA6 serum and maternal antibody play important roles in controlling CVA6 infection and viral replication. Collectively, these findings indicate that this neonatal murine model will be invaluable in future studies to develop CVA6-specific antivirals and vaccines.

IMPORTANCE Although coxsackievirus A6 (CVA6) infections are commonly mild and self-limiting, a small proportion of children may have serious complications, such as encephalitis, acute flaccid paralysis, and neurorespiratory syndrome, leading to fatalities. We have established a mouse model of CVA6 infection by inoculation of neonatal mice with a CVA6 clinical isolate that produced consistent pathological outcomes. Here, using this model of CVA6 infection, we found that high levels of IL-6 were associated with severe viral pneumonia and encephalitis, as in an evaluation of antiviral efficacy *in vivo*, IL-6 had no protective effect and instead accelerated death in neonatal mice. We demonstrated that, as antiviral drugs, both gamma interferon and ribavirin played important protective roles in the early stages of infection, with

Received 20 December 2016 **Accepted** 21 February 2017

Accepted manuscript posted online 1 March 2017

Citation Zhang Z, Dong Z, Wei Q, Carr MJ, Li J, Ding S, Tong Y, Li D, Shi W. 2017. A neonatal murine model of coxsackievirus A6 infection for evaluation of antiviral and vaccine efficacy. J Virol 91:e02450-16. https://doi.org/10.1128/JVI.02450-16.

Editor Julie K. Pfeiffer, University of Texas Southwestern Medical Center

Address correspondence to Dong Li, dli@tsmc.edu.cn, or Weifeng Shi, shiwf@ioz.ac.cn.

Z.Z. and Z.D. contributed equally to this work.

increased survival in treated neonatal mice challenged with CVA6. Moreover, active and passive immunization with the inactivated vaccines and anti-CVA6 serum also protected mice against homologous challenge infections.

KEYWORDS CVA6 infection, coxsackievirus, murine model, enterovirus

Human enteroviruses (EVs) are major pathogens in pediatric infectious disease and are classified into four species, EV-A to EV-D (1). Coxsackievirus A6 (CVA6) is a member of species EV-A, which currently comprises 16 serotypes, including 11 serotypes of coxsackievirus group A and five serotypes of EV (2–5). Prior to 2009, there were few reports of CVA6 epidemics and EV A71 (EVA71) and CVA16 were the major causative agents of hand, foot, and mouth disease (HFMD) worldwide. During the intervening years, large-scale outbreaks of CVA6 have been documented in Asia-Pacific regions, including Taiwan in 2009-2010 (6), Japan in 2011 (7), Thailand in 2012 (8), and Singapore in 2016 (9), where CVA6 even supplanted EVA71 and CVA16 as the predominant circulating serotype and was notably associated with severe illness and even fatalities (10, 11). In addition, in Europe and North America, CVA6 also caused sporadic infections from 2011 to 2015 (12–14), and cocirculated with CVA10 and CVB4 (15). In particular, CVA6 has become the predominant circulating serotype in mainland China (16–22). CVA6 clusters into five branches (lineages A to E), with two sublineages, E1 and E2 (23). Before 2011, lineage D, E1, and E2 strains cocirculated in Asia and Europe (6, 12, 24). Since 2008, E2 strains have become dominant and were responsible for HFMD outbreaks worldwide (23). Phylogenetic analysis based on the entire VP1 coding region of CVA6 showed that the epidemic strains in China and Finland belonged to the same clade (25). These findings indicate that the new CVA6 E2 sublineage circulates worldwide and has become one of the primary pathogens associated with HFMD.

In addition, most non-EVA71/CVA16 HFMD cases have caused only mild self-limiting symptoms (11). Clinical data indicate that symptomatic CVA6 infections do not occur in adults and are associated with a more severe disease course in children (26) than classical HFMD cases (13, 27). In addition, CVA6 infections could cause herpangina and onychomadesis during convalescence (28, 29). Recent reports have shown that CVA6 infections could also lead to serious acute complications in the central nervous system (CNS), such as aseptic meningitis, brainstem encephalitis (BE), and acute flaccid paralysis (30–33). Furthermore, coinfection with EVA71 and CVA6 was associated with serious CNS complications, and exacerbated disease (21, 34). Because of the disease severity associated with CVA6-associated infection, it represents a serious challenge to HFMD control, necessitating the development of new antivirals and prophylactic vaccines (23).

The type I, II, and III interferons (IFNs) are produced by leukocytes, fibroblasts, activated T lymphocytes, and NK cells in response to viral infection, which leads to the induction of antiviral pathways within hours. Therapeutically, IFN-α/β has been used for the treatment of hepatitis C virus infection and certain tumors (35). Yang and coworkers have shown a therapeutic effect of murine IFN-β on CVA16 infection in newborn mice (36). Liu et al. also found that IFN-α and IFN-ω play important roles in the control of EVA71 infection and replication, improved survival rates, and decreased the tissue viral titers in Institute of Cancer Research (ICR) mice after a virus challenge (37).

Currently, the pathogenesis of CVA6-associated HFMD is unclear. Furthermore, no licensed CVA6 vaccines are currently available and there are no effective anti-CVA6 drugs. In the present study, we established a neonatal mouse model of CVA6 infection for CVA6 vaccine and antiviral research and development. Furthermore, we used this model to explore the relationships among viral titers, inflammatory cytokines in different tissues, and disease severity and pathology. We also evaluated the efficacy of an inactivated CVA6 vaccine and antivirals in the control of CVA6 infection in a neonatal mouse model.

RESULTS

Establishment of a neonatal mouse model of CVA6 infection. Five-day-old ICR mice were divided into nine experimental groups and one negative-control group ($n = 10$ per group). The mice in three experimental groups were intramuscularly (i.m.), intraperitoneally (i.p.), and intracerebrally (i.c.) inoculated with an infective dose of 10^4 50% tissue culture infective doses ($TCID_{50}$), respectively. The average weights of the mice in the experimental groups infected with 10^4 $TCID_{50}$ of CVA6 strain WF057R were not significantly different from those of the mice in the negative-control group ($P > 0.05$, Fig. 1A to C). The mice showed transient symptoms with average clinical scores of <3 (Fig. 1D to F, mean value rounded to the nearest whole number), and the survival rates of the mice inoculated via the i.m., i.p., and i.c. routes were 30, 50, and 100%, respectively (Fig. 1G to I). These results indicated that 10^4 $TCID_{50}$ was unsuitable for the evaluation of CVA6 infection in the 5-day-old mouse model. The mice infected with $10^{5.5}$ $TCID_{50}$ via the i.c. pathway did not show a decreased average weight (Fig. 1A to C) but did show transient myasthenia, with an average clinical score of 2 (Fig. 1D to F). The average weights of the mice infected with $10^{5.5}$ $TCID_{50}$ through the i.m. and i.p. routes were significantly decreased at 9 days postinfection (dpi) by 51.47 and 22.42% (Fig. 1A to C), respectively, compared with the negative-control group. However, at this dose, there was a large variance and uneven distribution of clinical scores of the individuals treated via i.p. administration. Therefore, $10^{5.5}$ $TCID_{50}$ and 5-day-old mice were selected as the respective target dosage and age for infection as they began exhibiting clinical scores of 2 at 5 dpi (Fig. 1D to F). The average weight dropped rapidly, and the survival time was short for the mice infected with 10^7 $TCID_{50}$ of CVA6 via the i.m., i.p., and i.c. routes; hence, this dose was unsuitable for antiviral studies. We inoculated mice of different ages (3, 7, and 9 days) with $10^{5.5}$ $TCID_{50}$ i.m. The results showed that although the 3-day-old mice had obvious postinoculation symptoms and high clinical scores (Fig. 1J and K) and they were short-lived (Fig. 1L); the mortality rates of the 7- and 9-day-old mice were low and no clinical incidents or deaths were observed because of their older age (Fig. 1K and L). The average clinical scores of the 5-day-old mice i.m. inoculated with $10^{5.5}$ $TCID_{50}$ were 4 to 5, and all died between 6 and 11 dpi. The Mantel-Cox log rank test found that there was a statistically significant difference between the survival rates of 5-day-old mice and those of mice in the other age groups ($P < 0.001$). Therefore, $10^{5.5}$ $TCID_{50}$ was suitable for the i.m. inoculation of 5-day-old mice and the time of disease onset and mortality rate were stable and had good reproducibility.

Pathological changes in infected mice after an i.m. challenge with a lethal dose of CVA6. Although the time of disease onset was age and dosage dependent, the course of morbidity was very similar, with a slow progressive weight gain, followed by neurological symptoms, paralysis, and finally death. We inoculated 5-day-old mice with WF057R via i.m injection and analyzed the histopathological changes through hematoxylin-and-eosin (H&E) staining and immunohistochemical (IHC) analysis when the clinical scores reached the maximum (grade 5). Tissue samples taken from the brains, hearts, lungs, and hind limb skeletal muscles of mice at 5 dpi were subjected to pathology analysis. The results showed that there were multiple organ injuries and inflammatory responses in mice at later stages of infection. The encephalitis symptoms present in infected mice were similar to the neurological symptoms in humans; in the later stages of infection, inflammatory edema was present in the brain parenchyma (Fig. 2A). IHC analysis confirmed the presence of CVA6 antigen in the neural cells (Fig. 2B) and also indicated differences from CVA16 antigen, with no obvious pathological change or viral antigen found in the neurocytes of the brain. Severe viral myocarditis was observed, with myocardial lysis, microvesicular steatosis, capillary leak, and hypoxia in red blood cells at 5 dpi (Fig. 2E). At the same time, there was viral pneumonia, presenting as edema, sclerosis, and general lymphocytic infiltration in the lung parenchyma and the alveoli (Fig. 2I). The results showed that the hind limb skeletal muscle fibers exhibited severe necrosis and rupture (Fig. 2M); IHC analysis indicated that the

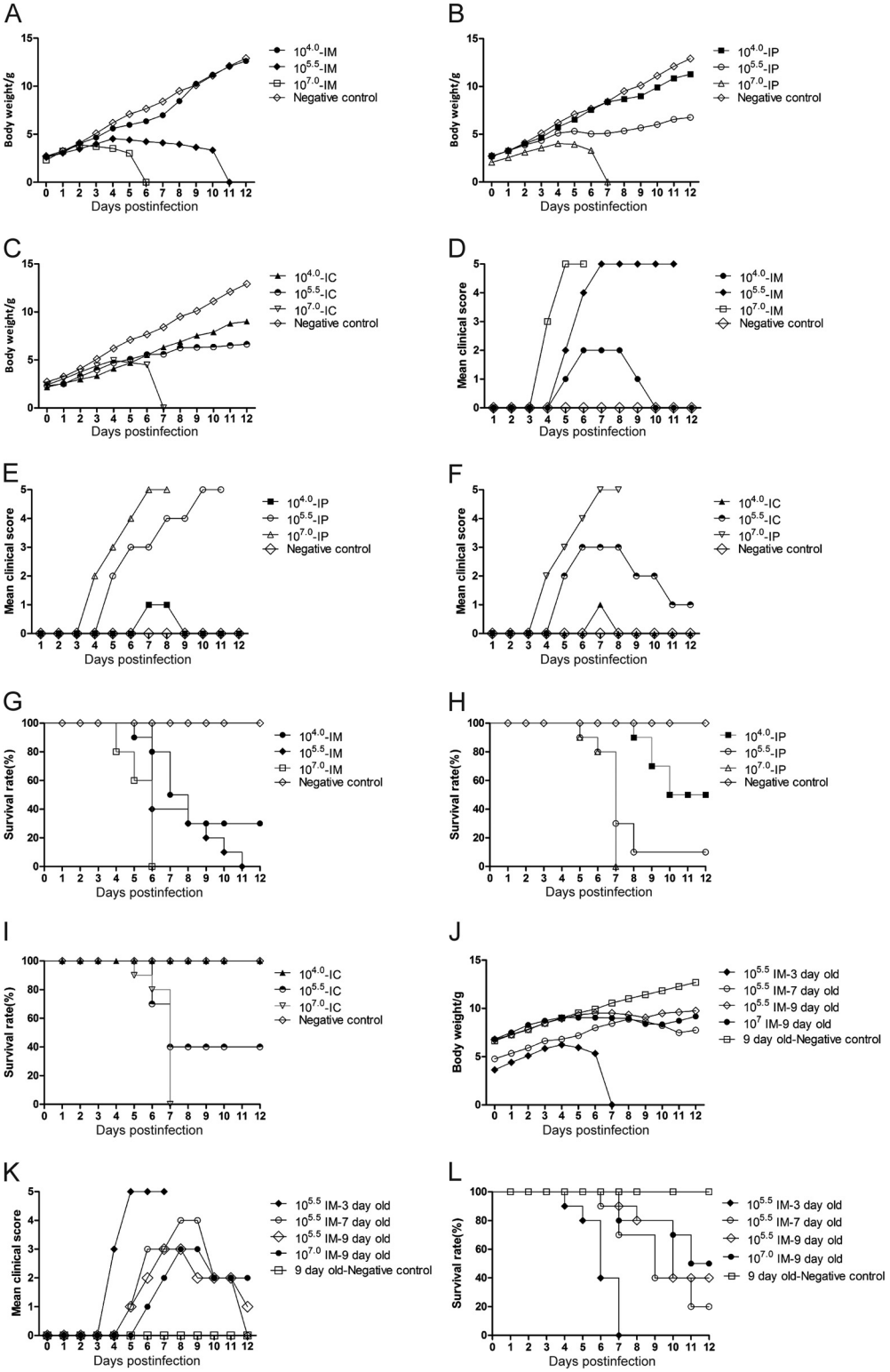

FIG 1 Body weights, clinical symptoms and survival rates of mice in the inoculation route-, dosage-, and age-dependent experiments. Five-day-old ICR mice ($n = 10$ per group) were i.c., i.m., and i.p. inoculated with different doses of WF057R (10^4, $10^{5.5}$, and 10^7 $TCID_{50}$/mouse), respectively. The LD_{50} was calculated as 1.02×10^3 $TCID_{50}$/mouse. A $10^{5.5}$ $TCID_{50}$/mouse (310 LD_{50}) challenge dose and the i.m. inoculation route were chosen. In addition, ICR mice ($n = 10$ per group) were i.m. inoculated with WF057R ($10^{5.5}$ $TCID_{50}$/mouse) at 3, 7, or 9 days of age, respectively. Control animals were administered culture medium instead of virus. The body weight (A, B, C, and J), clinical symptoms (D, E, F, and K), and survival rates (G, H, I, and L) were monitored and recorded daily after inoculation with CVA6 until 12 dpi. The Mantel-Cox log rank test was used to compare the survival rates of pups in different groups. Data represent the mean results of 10 mice ± the standard error of the mean. NC, negative control.

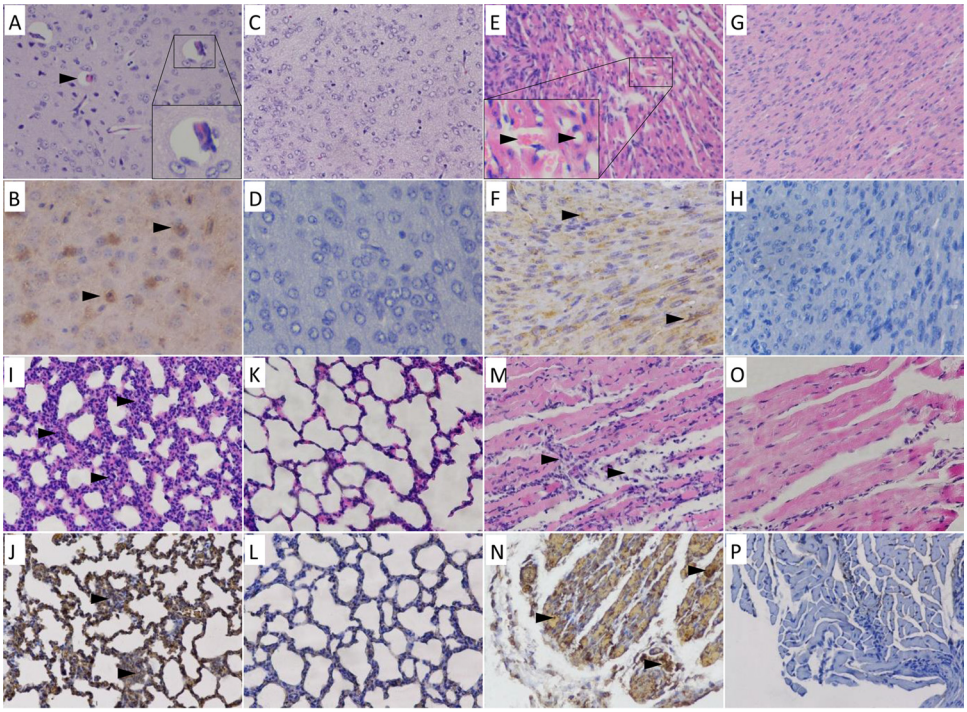

FIG 2 Histopathologic and IHC analyses of tissues from CVA6-infected neonatal mice. Five-day-old SPF ICR mice were i.m. inoculated with 310 LD_{50} of the WF057R strain or mock infected with MEM. Mice with grade 5 clinical symptoms infected with WF057R exhibited cerebral edema (A); severe myocardial lysis, microvesicular steatosis, capillary leakage, and hypoxia in red blood cells in the heart tissue (E); alveolar shrinkage and viral pneumonia in the lung tissue (I); and severe necrosis and loose muscle fibers in the hind limb muscle (M). IHC analysis indicated that the viral antigen was diffusely distributed in all of the isolated tissues (B, F, J, and N); there was no detectable antigen detected in the control group treated with the culture medium (D, H, L, and P). No histological changes were observed in brain, heart, lung, or hind limb muscle tissue samples of mock-infected mice (C, G, K, and O). Magnifications: B and D, ×400, other panels, ×200. All experiments were repeated three times.

viral antigen was diffusely distributed in the skeletal muscle fibers (Fig. 2N), and the viral titer was extremely high (11 $\log_{10}$ copies/mg). This was in agreement with the pathological injury to the lower limbs and with the clinical signs. Intestinal congestion and lymphocytic infiltration were observed during the late stage of infection (5 dpi), but intestinal necrosis was not. No pathological changes or viral antigen was detected in the spleens of WF057R-infected ICR mice. There were also no observable pathological changes or antigen detectable in the control group treated with the culture medium (Fig. 2C, D, G, H, K, L, O, and P).

Tissue viral loads in CVA6-infected mice. The viral loads in 5-day-old mice that were i.m. inoculated with $10^{5.5}$ $TCID_{50}$ were measured at 1, 3, and 5 dpi. The results showed that the viral loads differed significantly among tissues (Fig. 3). In general, there was a rapid increase in the viral load following infection from days 1 to 3 in all tissues in the early period and the rate of increase diminished by 5 dpi. The viral load in blood was <3 $\log_{10}$ copies/ml at 1 dpi; however, it increased to a maximum of 6.8 $\log_{10}$ copies/ml at 3 dpi. The time course of the viremia corresponded to the clinical presentation of the mice (including lethargy and weight loss). The viral loads in the heart and lungs reached 7 $\log_{10}$ copies/mg at 5 dpi. In the skeletal muscles, the viral loads reached 11 $\log_{10}$ copies/mg, 2 to 4 orders of magnitude greater than those in the other tissues and organs at all time points. This observation was consistent with the pathological changes and IHC staining results, indicating that CVA6 strain WF057R has strong muscle tissue tropism. The trend of the viral loads from 1 to 5 dpi in the different tissues of mice infected i.m. with 10^7 $TCID_{50}$ was similar to that of those infected with $10^{5.5}$ $TCID_{50}$, but the viral load was 1 to 2 $\log_{10}$ copies/mg greater (data not shown).

Cytokine levels in the peripheral blood of CVA6-infected mice 1 to 5 dpi. The expression of inflammatory cytokines in the peripheral blood was measured at 1 to 5

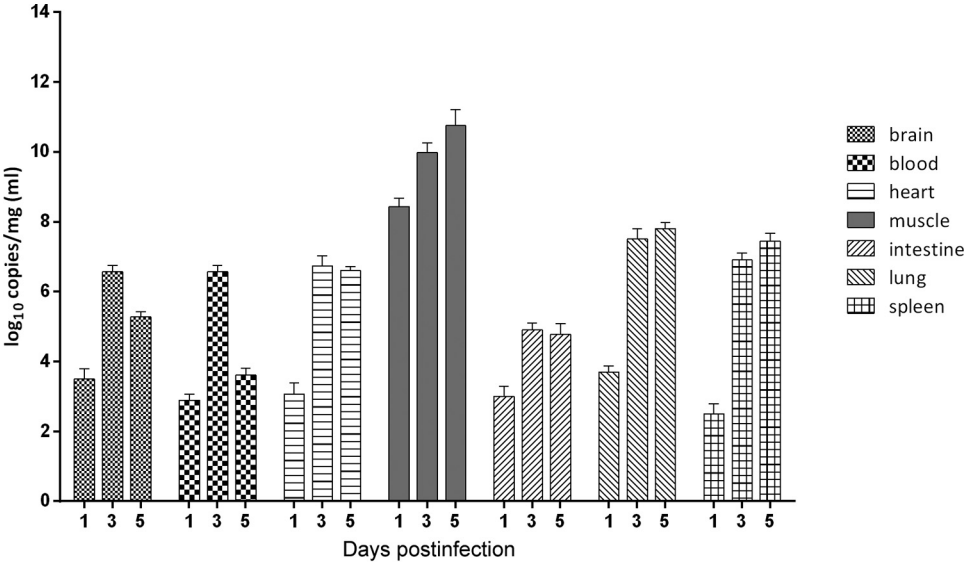

FIG 3 Virus titers in organs from mice infected with CVA6. Five-day-old ICR mice were i.m. inoculated with WF057R at $10^{5.5}$ $TCID_{50}$/mouse. At 1, 3, and 5 dpi, mice ($n = 3$) were euthanized and virus titers in the organs/tissues indicated were determined by quantitative reverse transcription-PCR (qRT-PCR). Results are expressed as numbers of viral RNA copies per milligram of tissue or milliliter of blood. Data represent the mean results of three mice ± the standard error of the mean.

dpi in 5-day-old ICR mice infected with CVA6 strain WF057R following infection with a lethal dose (310 50% lethal doses [LD_{50}]). The results showed that in the early stage of CVA6 infection, the expression of the cytokines IFN-γ, tumor necrosis factor alpha (TNF-α), IL-6, IL-10, IL-13, and IL-18 in the peripheral blood was significantly greater than that in the negative-control group ($P < 0.0001$, Fig. 4). The expression levels of IL-6 and IFN-γ showed an extremely sharp increase and peaked at 2,000 pg/ml, with a pattern of increase followed by a decrease in expression during the course of infection (Fig. 4A and B). The IL-10 expression level peaked at 39 pg/ml in the early period of infection (at 2 dpi) and then gradually decreased (Fig. 4C). IL-13 was also highly expressed in the early period, but the expression level dropped rapidly on subsequent days (Fig. 4D). In the later period of infection (at 5 dpi), the TNF-α level increased and reached 100 pg/ml (Fig. 4E). The expression of IL-18 in the entire infection course was not significantly different from that in the negative-control group (Fig. 4F). No IL-1β or IL-4 expression was detected (data not shown). These results showed that IL-6 and IFN-γ may be the major factors in early inflammatory responses during CVA6 infection in neonatal mice and that TNF-α, IL-10, and IL-13 may play important roles in the process of severe immunopathological injury.

Protective efficacy of IFNs and ribavirin against a CVA6 challenge *in vitro* and *in vivo*. To further characterize the antiviral effects of IFNs and ribavirin, we examined whether rhabdomyosarcoma (RD) cell lines were protected from CVA6-induced cell death *in vitro*. The cells were pretreated with IFN-α1b (125 U), IFN-α2a (125 U), IFN-β (12.5 U), IFN-γ (25 U), IFN-λ1 (125 U), IL-1β (1,250 U), and IL-6 (12.5 U) for 4 h before infection with CVA6 strain WF057R. Viral infections resulted in an easily discernible cytopathic effect (CPE) in RD cells, including necrosis and monolayer detachment, which decreased following pretreatment with different IFNs and ribavirin by inhibition of viral replication. The inhibitory effect on the rate of viral replication in RD cells was measured by Cell Counting Kit-8 (CCK-8) assay. The inhibitory rates of IFN-α1b, IFN-α2a, IFN-β, IFN-γ, and IFN-λ1 were 30.98, 27.37, 16.69, 25.34, and 3.20%, respectively, after CVA6 infection at 48 h postinfection (hpi) *in vitro* (Fig. 5A). The results showed that both type I IFNs (IFN-α1b and IFN-α2a) had higher antiviral activities than the type II and III IFNs (IFN-γ and IFN-λ1) *in vitro*. As reflected by a decreased inhibition rate (Fig. 5A), the survival rates of IFN-λ1-, IL-1β-, and IL-6-treated cells were lower following CVA6

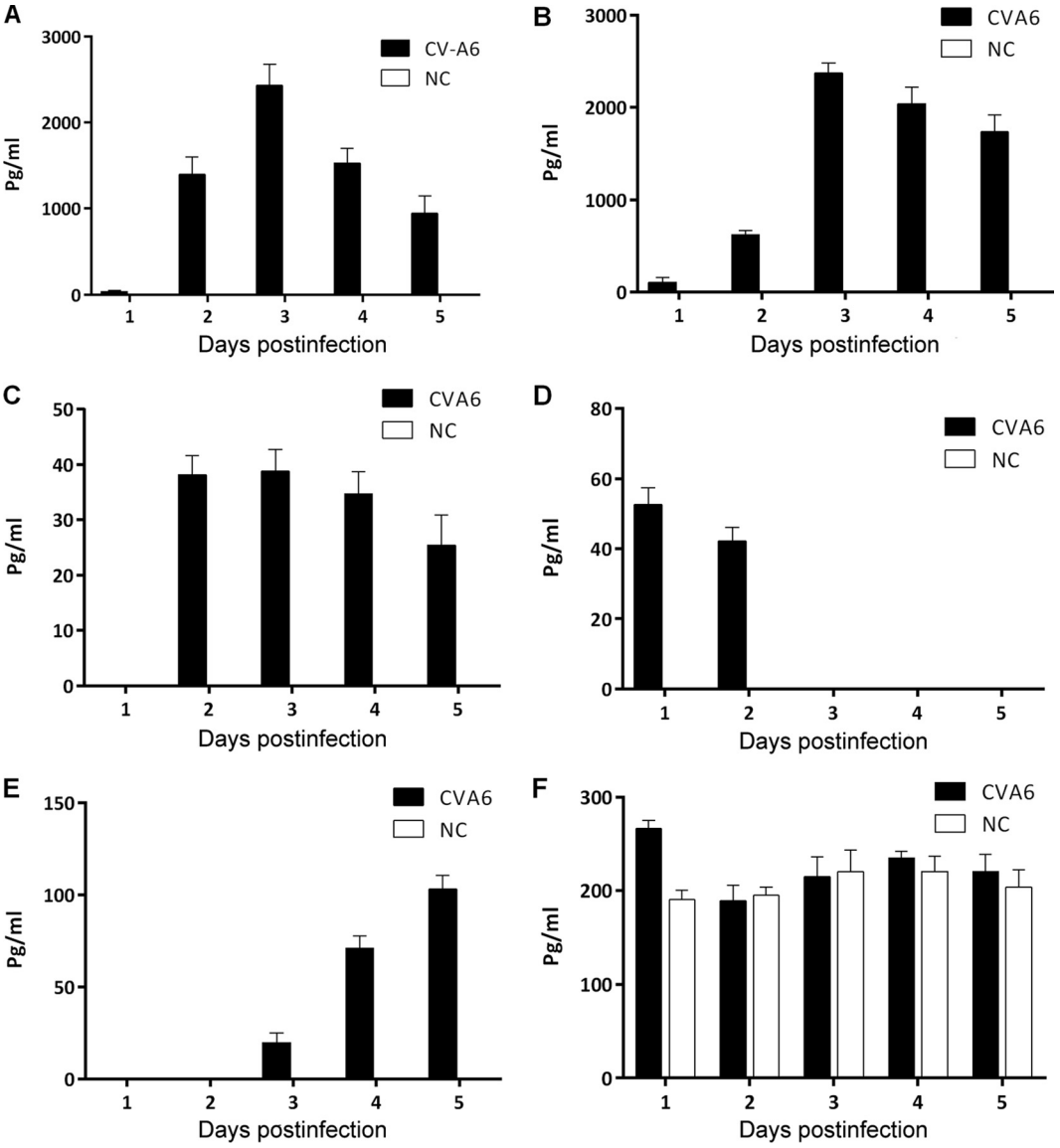

FIG 4 Expression of plasma proinflammatory cytokines in neonatal ICR mice infected with CVA6. The levels of IL-6 (A), IFN-γ (B), IL-10 (C), IL-13 (D), TNF-α (E), and IL-18 (F) in the plasma of 5-day-old ICR mice i.m. inoculated with a lethal dose of WF057R (310 LD_{50}) at 1, 2, 3, 4, and 5 dpi, were determined with individual mouse ELISA detection kits. No IL-1β or IL-4 expression was detected (data not shown). Data represent the mean results of three experiments $\pm$ the standard error of the mean. NC, negative control.

infection than those of cells treated with type I and II IFNs ($P < 0.05$). Furthermore, results of dynamic monitoring showed that the viral loads at 32, 40, and 48 hpi in the IFN-α1b, IFN-α2a, IFN-β, IFN-γ, and ribavirin intervention groups were significantly lower than those in the control group (Fig. 5B). Taken together, the results indicated that, compared to other IFNs and ribavirin, the type IIFNs (IFN-α1b and IFN-α2a) had higher antiviral activities against CVA6 *in vitro* in the early infection period.

IFNs and ribavirin were next employed in *in vivo* protection experiments. Five-day-old mice inoculated with lethal doses of CVA6 strain WF057R were injected with therapeutic doses of cytokines or ribavirin, respectively. The clinical symptoms of the mice were under active observation, and the mortality rates were determined. The control group that received no treatment showed obvious symptoms (Fig. 5C) and died in a short time. Unexpectedly, in contrast to the strong antiviral effect *in vitro* (the inhibition rate peaked at 30.98%), the antiviral activity of IFN-α2a against CVA6 *in vivo* was weak and the survival rates of the intervention mice were not significantly different

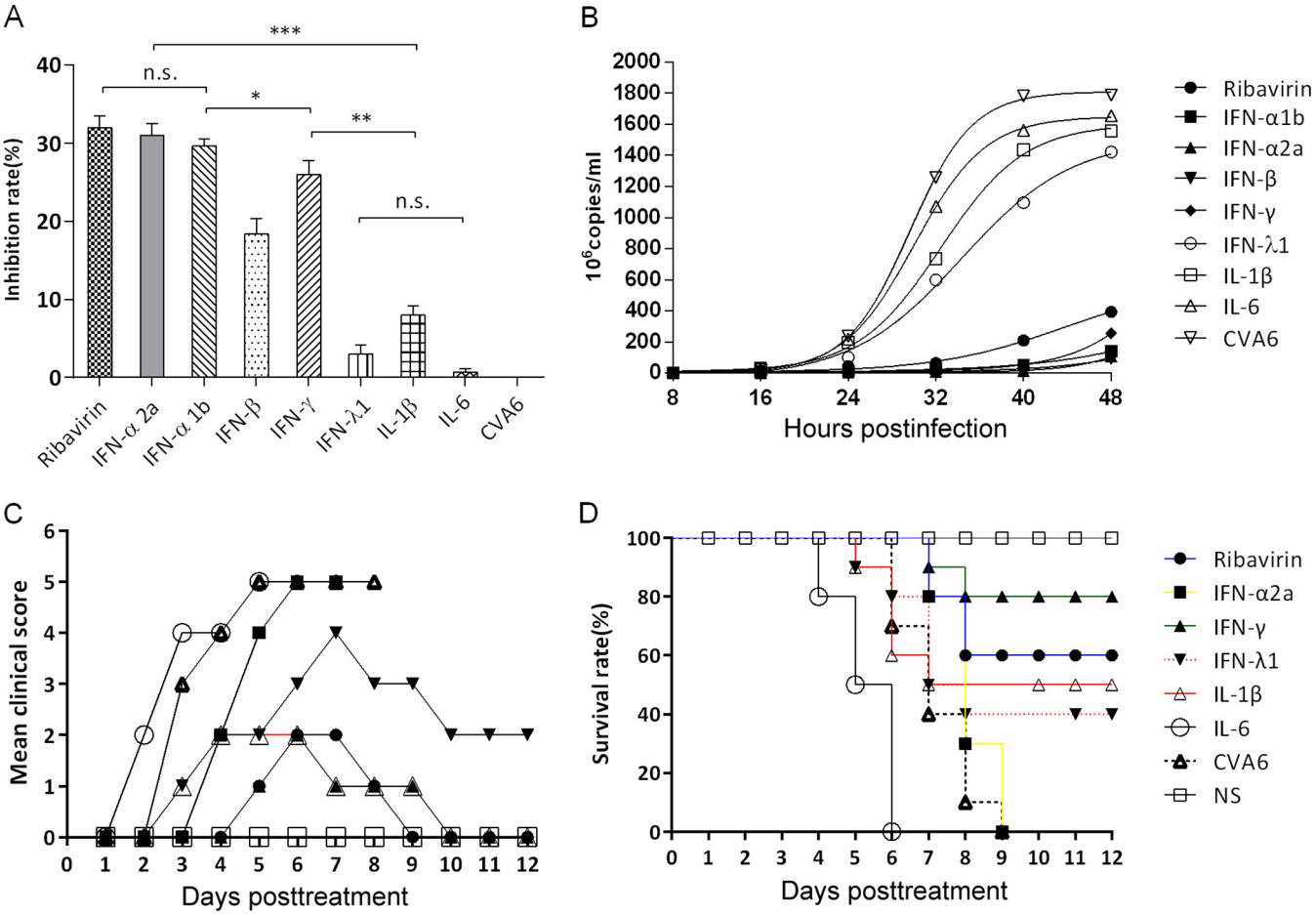

FIG 5 The inhibitory anti-CVA6 activities of ribavirin, IFN-α1b, IFN-α2a, IFN-β, IFN-γ, IFN-λ1, IL-1β, and IL-6 on CVA6 reproduction were evaluated *in vitro* and *in vivo*. (A) RD cells (5×10^5/well) were treated with different drugs for 4 h and then infected with WF057R at an MOI of 0.01. After the cells had been cultured for 24 h, the rate of viral inhibition was evaluated with a CCK-8 assay. The results shown are representative of three independent experiments. (B) During the infection of RD cells for 48 h with WF057R, 100 μl of culture medium from the experimental and control groups was taken at 8-h intervals and the viral loads in the supernatant were determined by qRT-PCR. Virus loads were expressed as the $\log_{10}$ number of copies per milliliter. The results shown are representative of three independent experiments. Clinical symptoms (C) and survival rates (D) were monitored and recorded daily after 5-day-old ICR mice ($n = 10$ per group) were i.m. challenged with lethal doses of WF057R (310 LD_{50}) until 12 dpi. Within 1 h postinoculation, each mouse was i.m. injected with different doses of cytokines (IFN-α2a, 666.75 U; IFN-γ, 833.25 U; IFN-λ1, 125 μg; IL-1β, 2,000 U; IL-6, 1,000 U; ribavirin, 100 μg). The Mantel-Cox log rank test was used to compare the survival rate of the pups in each drug treatment group with that of the medium control group. *, $P < 0.05$; **, $P < 0.01$; ***, $P < 0.001$ (one-way analysis of variance with Newman-Keuls multiple-comparison test); n.s., not significant; NS, negative serum.

from those of the nonintervention mice after inoculation with lethal doses (Fig. 5D). However, the clinical score of the IFN-γ- and ribavirin-treated groups was 2 and decreased at 8 dpi after inoculation (Fig. 5C), with final survival rates of 80 and 60% (Fig. 5D), respectively. Not only did treatment with IL-6 fail to have a protective effect, but it accelerated the deaths of neonatal mice (Fig. 5D), with a rapid onset of clinical symptoms and high clinical scores. By quantitative reverse transcription (qRT)-PCR, we did not detect viral RNA in the tissues of mice recovering from illness. The results suggested that IFN-γ and ribavirin afforded protection against lethal doses of virus *in vivo*.

Protective efficacy of virus antiserum and maternal antibody against a CVA6 challenge *in vivo*. First, microneutralization assays of CVA6 antiserum collected on day 7 after two immunizations with inactivated CVA6 strain WF057R were performed. The CVA6 antiserum in minimum essential medium (MEM) was 2-fold serially diluted in cultured RD cells *in vitro*, which were then inoculated with 100 TCD_{50} of virus. The viral antibody geometric mean titer (GMT), defined as the highest serum dilution at which at least two of the three replicates were CPE negative, was 1,024. To evaluate the protective efficacy of the neutralizing antiserum, 50 μl of the anti-CVA6 serum at

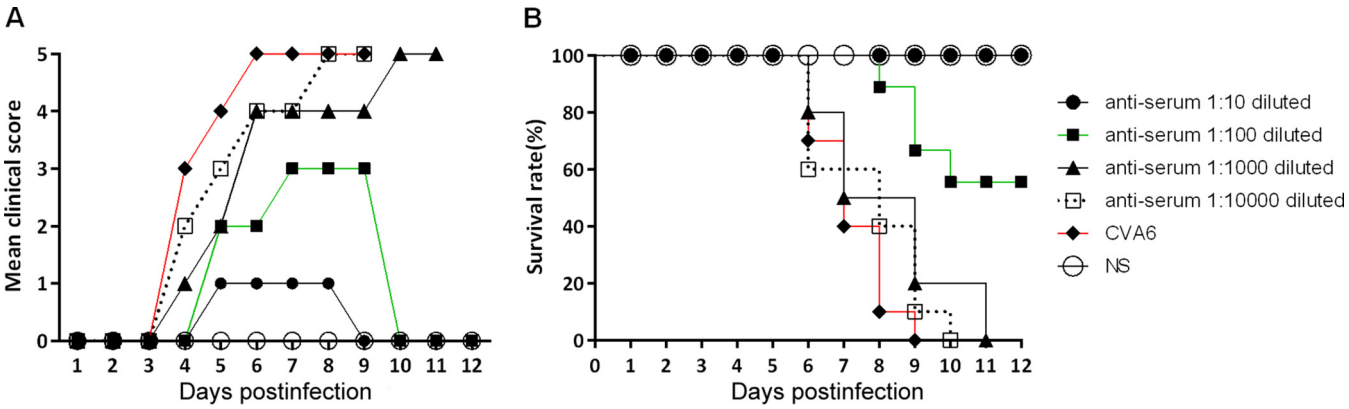

FIG 6 Passive immunization with CVA6 antiserum protected pups against a CVA6 challenge *in vivo*. First, 5-day-old ICR mice ($n = 10$ per group) were i.m. inoculated with 310 LD_{50} of strain WF057R. Within 1 h of inoculation, each mouse was i.m. inoculated with 50 μl of 10-fold serially diluted (10- to 10,000-fold) mouse CVA6 antiserum or negative serum (NS). Clinical symptoms (A) and survival rates (B) were then monitored and recorded daily for 12 days after inoculation with CVA6. The Mantel-Cox log rank test was used to compare the survival of the pups in each antiserum group and that of the pups in the medium control group at 12 dpi.

dilutions of 1:10, 1:100, 1:1,000, and 1:10,000 or the negative serum was passively transferred into suckling mice, followed by i.m. inoculation with 310 LD_{50} of CVA6. After the challenge, the mice that received negative serum exhibited disease at 3 dpi (grade 3), and finally all died by 9 dpi (Fig. 6A). In contrast, the majority of the mice given the lower dilutions of anti-CVA6 serum (1:10 to 1:100) were either completely or partially protected from paralysis and a fatal outcome, with survival rates of 100 and 60%, respectively (Fig. 6B). No protective effect was found at dilutions of 1:1,000 to 10,000, and at 10 dpi, all of the mice in these groups were dead. A 630-fold dilution of CVA6 antiserum can neutralize virus and protect 50% of the experimental animals (50% effective dose I [ED_{50}I] = 1.63) in the *in vivo* passive immunization test.

Second, we determined whether the maternal antibody induced by our CVA6 vaccine candidate could protect neonatal mice from a challenge with lethal doses of other CVA6 genotype E2 strains. Inactivated CVA6 strain WF057R and culture medium were used to i.m. immunize female adult mice three times at 1-week intervals, and they were allowed to mate 1 h after the first injection. The female mice delivered pups 5 to 10 days after the third inoculation. After delivery, the pups were i.m. challenged on day 5 with lethal doses of CVA6 clinical strain WF057R (310 LD_{50}), WH15066 (300 LD_{50}), DY003R (300 LD_{50}), DY005R (300 LD_{50}), or LW03R (300 LD_{50}). The neonatal mice born to unimmunized mothers in the four groups started to die an average of 9 days after virus inoculation, almost no weight gain was observed, and all were dead by 11 dpi (data not shown). In contrast, newborn mice born to dams immunized with inactivated WF057R had the fastest weight gain and were without clinical symptoms (Fig. 7A). Newborn mice of mothers immunized with the vaccine candidate had a 100% survival rate after inoculation with different local strains of CVA6 (Fig. 7B). These results suggested that our inactivated CVA6 vaccine candidate offers high efficacy and broad-spectrum cross-protection against diverse CVA6 isolates in the neonatal mouse model.

Therapeutic effect of CVA6 antiserum. To confirm the therapeutic effect of the CVA6 antiserum on disease incidence, we treated neonatal mice with differing disease severities (in early or late stages) via i.v. injection with a serum dilution series (1:1, 1:10, and 1:50). The results of this treatment experiment showed that the clinical symptoms in the early stages (grade 1 to 2) gradually disappeared, the clinical score concomitantly decreased (Fig. 8A), and there was a gain in body weight in the treated group. The protective indices of antiserum at different dilutions (1:1, 1:10, and 1:50) were 100, 100, and 40% (Fig. 8B), respectively. Overall, 10 mice in every treated group had clinical symptoms such as transient paralysis of the hind limbs during treatment; >40% of them recovered. Ten neonatal mice (grade >3) exhibited nervous system involvement with paralysis of one or both hind limbs and even death, which indicated a lack of

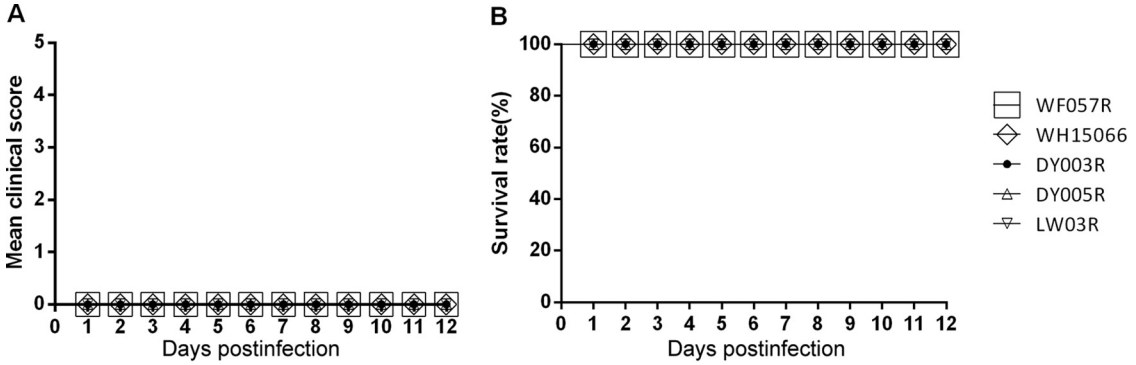

FIG 7 Maternal immunization with inactivated whole-virus CVA6 antigen protects pups against lethal challenge doses of various CVA6 strains. Eight-week-old female ICR mice (n = 4 per group) were i.m. injected twice 2 weeks apart with 50 μl of the formaldehyde-inactivated CVA6 vaccine or medium. The mice were allowed to mate after the first immunization. Mice immunized with MEM were used as controls. The pups were i.m. challenged with lethal doses of the following CVA6 strains: WF057R (310 LD_{50}), WH15066 (300 LD_{50}), DY003R (300 LD_{50}), DY005R (300 LD_{50}), and LW03R (300 LD_{50}) on postnatal day 5. The body weights, clinical symptoms (A), and survival rates (B) of the challenged pups were monitored as described above until 12 days after inoculation. The Mantel-Cox log rank test was used to compare the survival of pups in each antiserum group and that of the pups in the medium control group at 12 dpi.

efficacy of the antiserum treatment compared to that in the untreated group. The neonatal mice in the treated group were all dead at 9 to 11 dpi (Fig. 8B). A 43-fold dilution of anti-CVA6 serum can neutralize virus and protect 50% of the experimental animals (ED_{50}II = 23.81) in the *in vivo* therapeutic test.

DISCUSSION

Several animal models have been developed for the evaluation of EVA71 and CVA16 vaccine candidates (38–43). Because of the upsurge in epidemic HFMD attributable to CVA6 in the last 5 years, there is an urgent need to investigate alternative models. Yang and coworkers have recently published a CVA6 murine model (44) for the study of vaccines and pathogenic mechanisms. The two CVA6 murine models, however, differ in a number of important respects, i.e., the dose and route of inoculation, the ages and strains of the laboratory mice employed, and also, critically, the viral strain employed. First, we tested three different inoculation routes, i.c., i.m., and i.p., and selected i.m. inoculation to construct the mouse model. In comparison, Yang et al. also tried three different inoculation routes, i.c., i.p., and intragastric, and used the i.p. route (44). However, we found that i.m. inoculation was superior to i.p. inoculation in that mice inoculated i.p. had significant variations in clinical scores and times of death. On the contrary, the clinical outcomes of mice treated via the i.m. route were more consistent.

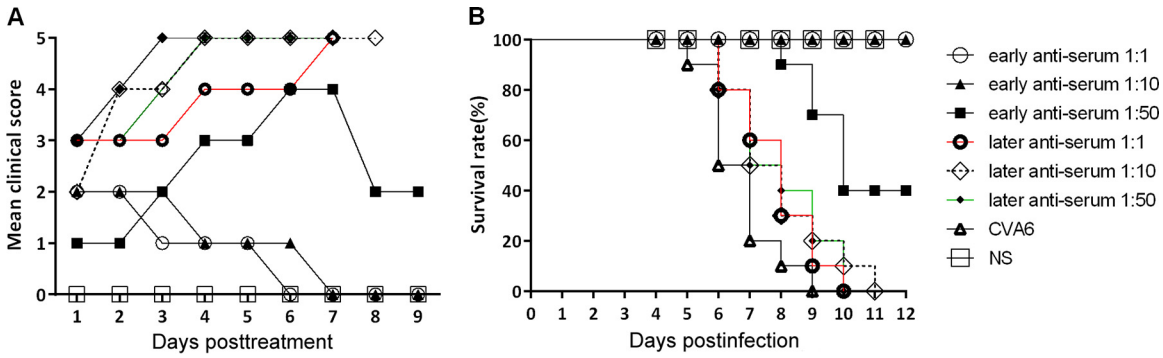

FIG 8 Therapeutic effect of the administration of CVA6 antiserum on symptoms and survival rate of neonatal mice *in vivo*. Five-day-old ICR mice were i.m. inoculated with 310 LD_{50} of WF057R, which result in a 100% mortality rate. The mice in early (grade 1 to 2) and late (grade >3) infection stages were selected and divided into six experimental groups (n = 10 per group). The mice in the experimental groups were i.v. injected with 50 μl of different dilutions (1-, 10-, and 50-fold) of mouse CVA6 antiserum and negative serum (NS), respectively. Their clinical symptoms (A) and survival rates (B) were then monitored and recorded daily for 12 days after inoculation with CVA6. The Mantel-Cox log rank test was used to compare the survival of the pups in each antiserum group and that of the pups in the medium control group at 12 days postinoculation.

Second, compared to the BALB/c strains employed by Yang and colleagues (44), ICR neonatal mice are more susceptible to CVA6 infection. For example, 5-day-old BALB/c mice inoculated with 10^5 or 10^6 $TCID_{50}$ of CVA6 i.p. have a survival rate of 100%, with a clinical score of 0 (44). In contrast, 100% of the 5-day-old ICR neonatal mice inoculated with CVA6 by the same i.p. route died by 11 dpi and furthermore, the mice had clinical symptoms (grade 5). Third, 5-day-old neonatal mice were also used in our study, as opposed to the 1-day-old mice employed in the previous work. Finally, the strains we employed were isolated in 2013 to 2015, coincident with the upsurge in CVA6-associated disease, and were genetically highly related to other prevalent Chinese CVA6 circulating strains (>98% identity). In contrast, the CVA6 strain employed by Yang et al. was isolated in Taiwan in 2007 (45) and the homology between this strain and the prevalent strains circulating in China over the same period was 91%. All of the five Shandong CVA6 strains employed in the present study are highly virulent in *in vitro* and *in vivo* pathogenicity experiments and are associated with HFMD in children, as is the Taiwanese strain, and further work is required to investigate strain-specific differences in pathogenicity.

Pathological sectioning and IHC tests showed that CVA6 had a strong tropism for musculoskeletal tissues and proliferated rapidly therein, which was associated with muscle necrosis and muscle bundle rupture. This could be one of the direct causes of limb paralysis in neonatal mice, and this pathological feature was similar to that previously reported for EVA71 and CVA16 (40, 41). The lethal edema of the cardiac tissues in the late infection time period could be an accelerating factor in the death of CVA6-infected mice. This observation was in agreement with the investigation of severe clinical cases of patients who died of myocardial pathology (46). In addition, there was only limited hyperemia and lymphocytic infiltrates in the gastrointestinal regions, and no necrosis was observed, which is an additional differentiating feature compared to reports of EVA71 animal models (47, 48) and this distinguishing clinical feature might be attributable to the infection pathway.

Inoculation of CVA6 strain WF057R by the i.m. and i.p. routes produced extremely high viral titers in skeletal muscles of >10 and 7 $\log_{10}$ copies/mg, respectively, that were significantly greater than those in other organs (2 to 4 $\log_{10}$ higher titers), indicating that hind limb muscle is the most active site of viral replication. Lin et al. found that the muscle cells in EVA71 receptor hSCARB2 transgenic mice have the greatest loads of EVA71 (4.5×10^6 PFU), whereas the muscle tissues in the non-receptor-expressing mice had only basal replication of EVA71 (49). Similarly, CVA16 titers were found to be highest in muscle tissues of neonatal mice (10^7 $\log_{10}$/mg) (42). Via the i.m. inoculation route, infection of leukocytes may infiltrate the brain parenchyma, and also, retrograde transmission up peripheral motor nerves that highly innervate skeletal muscles leads to systemic infection, as seen in an i.m. model of EVA71 encephalomyelitis (50, 51). Inoculation by the i.m. route produced more severe pathological T lymphocyte tissue infiltration, potentially resulting in abnormal expression of systemic inflammatory cytokines/chemokines, leading to neuropathology during viral infection (52).

The role of viral versus immunological factors in CVA6 pathogenesis has been extensively discussed; it has been proposed that overwhelming virus replication combined with the induction of massive quantities of proinflammatory cytokines contributes to the severity of viral infection (53, 54). Indeed, high levels of several cytokines/chemokines were associated with human BE and pulmonary edema in EVA71 infections in previous studies (55–58). Similarly, our data showed that 3 days after mice were inoculated with CVA6, there was a dramatic increase in IL-6 and IFN-γ levels in the peripheral blood, which was similar to that seen in humans, accompanied by injuries likely due to rapid viral replication. These factors were potentially the major causes of severe viral pneumonia and encephalitis, and in mice, IL-6 was reported to be pathogenic in bacterial sepsis and meningitis, as well as during influenza infection (59). Indeed, anti-IL-6 antibody-treated mice displayed less tissue damage than untreated EVA71-infected controls and an absence of vascular pathology (47). As for the similar-

ities between HFMD BE patients and the neonatal mouse model, notably, after neurons were infected with the virus, the IFN-γ expression level was increased, potentially leading to inhibition of IL-4 secretion by Th2 cells and thereby causing an imbalance in the IFN-γ/IL-4 ratio. The inflammatory and immunologic overresponses that occurred when clearing virus-infected cells were the leading factors associated with severe cases (53, 60, 61). The mechanism(s) of specific immunologic injury in CVA6-infected neurons merits further investigation.

Thus far, there is no effective treatment regimen for HFMD and only i.v. immunoglobulin has been licensed as an anti-EVA71 therapy; however, its efficacy is undemonstrated (58, 62). In the present study, ribavirin suppressed viral replication to extremely low levels *in vitro* ($<$5%) with a 60% survival rate *in vivo* and significantly shortened the duration of the disease. Similarly, groups pretreated with a clinically therapeutic dose of IFN-α2a (1,250 U/ml) showed suppression of CVA6 replication *in vitro* but antiviral activity *in vivo* was completely absent. Unlike the *in vitro* tests, IFN-γ showed antiviral efficacy and promoted an increase in the survival rates of infected 5-day-old mice. Our observations are not in agreement with studies on other EV species A members, possibly reflecting serotype-specific differences; for example, early administration of IFN-α2a in the treatment of EVA71-induced CNS infection can reverse injury to the nervous system (63). However, the likely participation of cytokines in the pathological process in the early stage of infection engenders caution in use of cytokine therapy. McConnell (64) has reported a vast difference in the protective effects of therapy if IFN is given at different times. If IFN therapy is started 3 days after EVA71 infection, it exacerbates clinical symptoms in neonatal mice. Therefore, cytokine therapy should potentially only be applied in the early stages of viral infection. Nonetheless, far more extensive studies of clinical efficacy and safety evaluations are needed to determine if ribavirin or IFN antiviral therapies can be used singly or in combination for the treatment of severe CVA6 infections.

Immunization is considered to be the most effective tool with which to control HFMD epidemics. However, experimental EVA71 and CVA16 vaccines could not induce heterologous cross-protection against infection with CVA6 (38). It is important for the development of a CVA6 vaccine to verify that anti-CVA6 serum has protective functions *in vivo* similar to those of EVA71 and CVA16 antisera. In the present study, high neutralizing titers (GMT = 1,024) were achieved shortly (1 week) after two immunizations at weeks 8 and 10. We used this immunization schedule to vaccinate adult female mice to determine if candidate vaccines can induce sufficiently high levels of expression of protective neutralizing antibodies and whether immunized adult female mice can transfer protective neutralizing antibodies on to their progeny. The same strategy has been successful in evaluating the protective efficacy of inactivated CVA16 vaccine candidates in mice (41), in which CVA16 neutralizing titers were obtained within a 2-week immunization schedule. Indeed, our results showed that immunization with inactivated CVA6 could elicit virus-specific protective antibody responses in mice. Furthermore, the CVA6 antiserum was able to inhibit the CPE induced by CVA6 *in vitro*; 0- and 100-fold dilutions of antisera were also both able to provide mice 100% protection against a lethal viral challenge, indicating that neutralizing antibodies may play an essential role in *in vivo* protection.

Our data demonstrate that the CVA6 antiserum neutralized four clinical isolates from different local regions and a mouse-adapted CVA6 strain, suggesting that the antiserum may strongly neutralize currently circulating E2 genotype strains. However, more CVA6 clinical isolates and genotypes need to be examined to determine the extent of neutralization by the CVA6 antiserum. The CVA6 antiserum did not neutralize EVA71 and CVB4 (Fig. 9), and reciprocally, antiserum against inactivated EVA71 or CVB4 did not appear to neutralize CVA6 (unpublished data). These results underscore the likely need for separate antigens for CVA6, EVA71, and CVB4 vaccines or, alternatively, to consider whether a CVA6-derived antigen should be combined with the corresponding EVA71 and CVB4 antigens to formulate a trivalent vaccine for protection against different HFMD agents.

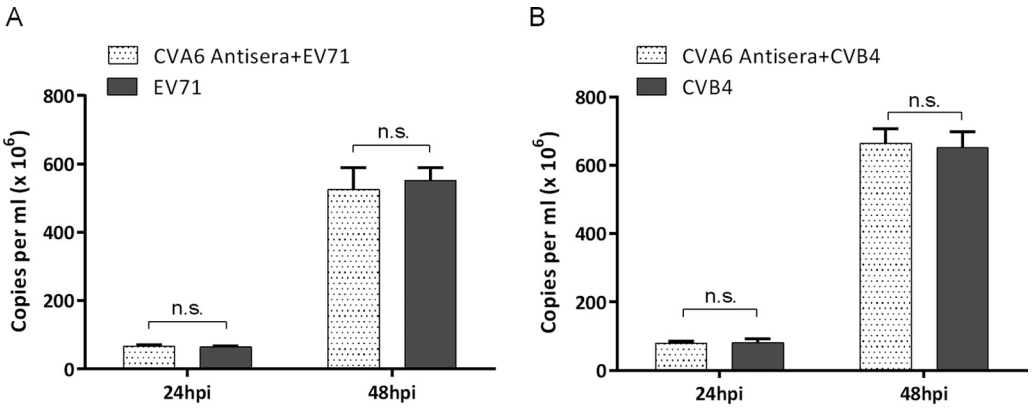

FIG 9 Examination of heterologous cross-protection of CVA6 antiserum. EVA71 or CVB4 pretreated *in vitro* with CVA6 antiserum showed no reduction in CPE in RD cells. RD cells (5×10^3/well) were plated on 96-well plates, grown overnight to >80% confluence, and then separately primed with 50 μl of CVA6 antiserum (neutralizing antibody GMT = 1,024) for 2 h before the addition of 50 μl of fresh medium containing 100 $TCID_{50}$ of EVA71 and CVB4 (MOI = 0.01). One-hundred-microliter volumes of culture medium were taken from the experimental and control groups at 24 and 48 hpi, and then the viral loads in the supernatant were determined by qRT-PCR to evaluate the effects of CVA6 antiserum on EVA71 (A) and CVB4 (B) replication. Virus loads are expressed as the number of copies per milliliter of cell supernatant. n.s., not significant.

The pathology associated with CVA6 infection progressed rapidly when severe complications and neurologic symptoms occurred. Conceivably, antibody treatment of CVA6-associated HFMD in the early stages could ameliorate disease severity. The data in the present study demonstrated that a 10-fold dilution of CVA6 antiserum was able to provide 100% protection in neonatal mice with grade 2 clinical scores following a challenge and also to prevent symptoms and disease severity from progressing. However, no protective effects or diminution of disease severity could be provided to neonatal mice with paralysis of the one or both hind limbs. On the basis of the murine infection model, the nervous system in neonatal mice (grade >3) exhibiting severe injury and systemic inflammatory responses has already been damaged by cerebral edema (Fig. 2A). The viral burden was >10 $\log_{10}$ copies/mg in the hind limbs, with apparent necrosis of skeletal muscle fibers and fracture (Fig. 2M). Therefore, it is likely difficult for neonatal mice to recover from severe disease. Following early intervention with therapy in mice challenged with CVA6, the outcome was significantly different from that in the nontreated group ($P < 0.005$), with the animals receiving treatment recovering without discernible sequelae.

On the basis of these findings, we conducted a thorough pathological analysis of the vaccinated neonatal mice. We paid special attention to the study of the immunologic injury in the vaccinated animals after a challenge. The results showed that when the histopathology was examined at different challenge time points, no changes were observed in the major organs, except for scant inflammatory cell infiltrations in the lungs and the bronchus. The results strongly suggested that the immunoprotection in the vaccinated ICR mice could lead to complete suppression of viral proliferation, hence affording protection against infection-induced pathological injury.

In conclusion, we have employed a clinical isolate to develop a CVA6 neonatal mouse model for evaluation of the therapeutic effects of different antivirals and the protective efficacies of vaccines. This model was demonstrated to be both robust and reproducible in terms of survival rates. Pathological observations, IHC staining, and quantitative reverse transcription-PCR (qRT-PCR) revealed that the CVA6 WF057R strain had a strong tropism for skeletal muscle and lung tissues, causing severe necrosis. Our data indicate that both IFN-γ and ribavirin can afford protection in the early stages of infection of neonatal mice challenged with lethal doses of CVA6. High levels of IL-6 were likely the major cause of severe viral pneumonia and encephalitis, as in an *in vivo* evaluation of antiviral efficacy, IL-6 offered no protection and instead accelerated death in neonatal mice. Using an antiserum protection study, a maternal antibody protection

study, and the antibody therapeutic test, we demonstrated that the specific CVA6 neutralizing antibody inhibited circulating CVA6 clinical isolates and showed the protective efficacy of a CVA6 vaccine in neonatal mice. Immediate CVA6 antiserum therapy should be considered for CVA6 cases following an early indication of neurological involvement.

MATERIALS AND METHODS

Ethics statement. Specific-pathogen-free (SPF) ICR mice (Charles River Lab Animal Technology Co., Ltd., Beijing, China; permission no. SCXK [Jing] 2012-0001) were employed to develop an animal model. The animal experiments described here were approved by the Taishan Medical College Administrative Committee for Laboratory Animals (permission no. 2016060) and complied with the guidance of the Shandong Laboratory Animal Welfare and Ethics of Shandong Administrative Committee of Laboratory Animals.

Viruses and cells. Human RD cells were cultured with Dulbecco's modified Eagle's medium supplemented with 2% fetal bovine serum plus 100 IU of penicillin and 100 μg of streptomycin per ml at 37°C in the presence of 5% CO_2. A CVA6 clinical isolate, WF057R, was isolated from a cerebrospinal fluid sample from a 2-year-old boy with HFMD during an outbreak in Shandong in 2014. All viruses were propagated and titrated in RD cells. Viral RNA was extracted from the CVA6 WF057R isolate, and RT-PCR and direct sequencing by standard methods were employed to obtain the full-length genome sequence. The titers of CVA6 were expressed in $TCID_{50}$ in accordance with the method of Reed and Muench (65). All CVA6 stocks were subjected to three freeze-thaw cycles, clarified by centrifugation at 4,000 $\times$ *g* for 10 min at 4°C, filtered through a 0.2-μm syringe filter (Pall Corporation, Germany), and stored at −80°C.

Experimental animal infections. Five-day-old mice ($n = 10$ per age group) were employed in the inoculation route-dependent, dose-dependent, and LD_{50} experiments with i.c., i.m., and i.p. inoculations with 10^4, $10^{5.5}$ and 10^7 $TCID_{50}$/animal, respectively. In age-dependent experiments, mice at 3, 7, and 9 days of age were selected ($n = 10$ per age group) and i.m. inoculated with WF057R (10^5 $TCID_{50}$/mouse). Control mice were administered uninfected culture medium and kept in a separate cage from the infected mice. Mice were observed daily for clinical illness, weight trends, and death until 12 days postinoculation. The grade of clinical disease was scored as follows: 0, healthy; 1, lethargy and inactivity; 2, hind limb weakness; 3, single limb paralysis; 4, double hind limb paralysis; 5, death (38). The LD_{50} was calculated by using the Reed and Muench formula (65).

Histopathologic and IHC staining. Five-day-old ICR mice were i.m. inoculated with WF057R (310 LD_{50}) or uninfected culture medium. At 5 and 6 dpi, experimental animals (grades 3 to 5, $n = 3$) and control animals (grade 0, $n = 3$) were euthanized and histopathologic and IHC examinations of tissues were performed. After anesthetization, brains, hearts, lungs, spleens, intestines, and contralateral hind limb skeletal muscles (other than those inoculated) were collected and fixed in 10% neutral buffered formalin for at least 2 days. Tissues were then bisected and embedded in paraffin. For histopathologic examination, tissue sections were stained with H&E.

For IHC testing, tissue sections were dewaxed, dehydrated, and microwaved for 14 min at 92 to 99°C in citrate buffer. Polyclonal mouse anti-CVA6 antibody (1:100 dilution) was applied for 1 h at 37°C. A peroxidase-conjugated secondary antibody (1:1,000 dilution; Origene, Beijing ZhongshanGoldenBridge Biotechnology Development Co., Ltd., Beijing, China) was added for 30 min of incubation at room temperature, which was followed by addition of the chromogen 3,3′-diaminobenzidine tetrahydrochloride (Beyotime; Shanghai Beyotime Biotechnology Development Co., Ltd., Shanghai, China). Tissues were counterstained with hematoxylin. Control sections were incubated with normal mouse serum instead of anti-CVA6 antibody.

Viral titers in mouse tissues. After i.m. inoculation with WF057R ($10^{5.5}$ or 10^7 $TCID_{50}$/mouse) or uninfected culture medium, viral loads were measured in nine experimental and three control ICR mice as follows. Blood, brains, hearts, lungs, spleens, intestines, and contralateral hind limb skeletal muscles (other than those inoculated) were aseptically removed, weighed, and stored at −80°C. Tissue and blood samples from experimental mice ($n = 3$ per time point) were collected at 1, 3, and 5 dpi. Samples from control mice ($n = 3$) were collected at 0 dpi. The tissue samples were homogenized in sterile phosphate-buffered saline (10%, wt/vol), disrupted by three freeze-thaw cycles, and centrifuged. Total RNA was extracted from individual organs/tissues of infected mice with TRIzol reagent (TaKaRa, Dalian, China) and reverse transcribed with random hexamers and Moloney murine leukemia virus reverse transcriptase (TaKaRa, Dalian, China) to generate cDNA in accordance with the manufacturer's instructions. The resulting cDNA was employed for real-time PCR with a GoldStarTaqman Mixture kit (CWBIO, Beijing, China) and the oligonucleotide primers 5′-CCTGAATGCGGCTAATCC-3′ (forward) and 5′-TTGTCACCATW AGCAGYCA-3′ (reverse) and the probe 5′–6-carboxyfluorescein–CCGACTACTTTGGGWGTCCGTGT–Black Hole Quencher 1–3′ (66). Real-time PCRs were carried out for 40 cycles of 95°C for 15 s and 60°C for 60 s on the 7500 Fast System (Applied Biosystems). Viral loads were expressed as the $\log_{10}$ number of copies per milligram of tissue or milliliter of blood. A standard curve was used to quantify the viral RNA in each serum sample. The standard curve was generated from serially diluted plasmid pMD18-CV, ranging from 10^8 to 10^1 copies/ml (67). Cutoff threshold cycle values were determined from negative controls with normal mouse serum. A standard curve correlation coefficient of >0.995 and a PCR efficiency of $>90\%$ were used as assay acceptance criteria.

Cytokine assays. Levels of the proinflammatory cytokines IL-1β, IL-6, IL-18, and TNF-α; that of the anti-inflammatory cytokine IL-10; and those of the chemokines IL-4, IL-13, and IFN-γ in plasma of 5-day-old ICR mice i.m. inoculated with lethal doses of WF057R (310 LD_{50}) at 1, 2, 3, 4, and 5 dpi were

determined with individual mouse enzyme-linked immunosorbent assay (ELISA) detection kits (Multisciences Biotechnology Co., Ltd., Hangzhou, China) in accordance with the manufacturer's instructions. The results are presented as mean values derived from duplicate tests. The theoretical limits of detection were as follows: IL-1β, 1.03 pg/ml; IL-6, 1.17 pg/ml; IL-18, 0.21 pg/ml; TNF-α, 1.63 pg/ml; IL-10, 1.17 pg/ml; IL-4, 0.22 pg/ml; IL-13, 1.17 pg/ml; IFN-γ, 1.74 pg/ml.

***In vitro* and *in vivo* ribavirin and cytokine antiviral activity assays.** Antiviral activity was evaluated on RD cells *in vitro* with a CCK-8 assay (Multisciences Biotechnology Co., Ltd., Hangzhou, China) to examine the effects of cytokines and ribavirin on viral multiplication. RD cells (5×10^3/well) were plated on 96-well plates, grown overnight to >80% confluence, and then separately primed with human IFN-α1b (1,250 U/ml), IFN-α2a (1,250 U/ml), IFN-β (125 U/ml), IFN-γ (250 U/ml), IFN-λ1 (1,250 ng/ml), IL-1β (12,500 U/ml), and IL-6 (125 U/ml). A separate well contained ribavirin (8.19×10^{-5} mol/liter) and a negative control with MEM. Cells were precultured for 4 h before the addition of 50 μl of fresh medium containing 100 $TCID_{50}$ of WF057R (multiplicity of infection [MOI] of 0.01). After being cultured for 24 h in a 5% CO_2 atmosphere at 37°C, the cell supernatant was washed three times with phosphate-buffered saline (pH 7.4) and incubated with 100 μl of 10% CCK-8 solution per well for 1.5 h. The absorbance at 450 nm was then measured spectrophotometrically with a microplate reader (ELX-800; BioTek). Untreated cells represented a 100% cell viability control, and the medium served as a background reference. Percent survival was calculated by comparison of treated samples with the control by subtracting the background reference with the equation $SP\ (\%) = [(A - A_1)/(A_2 - A_1)] \times 100\%$, where *SP* (%) represents percent survival and A, A_1, and A_2 are the absorbances of the sample, background, and control wells, respectively. In other experiments, RD cells were infected with WF057R for 48 h, 100 μl of culture medium was taken from the experimental and control groups at 8-h intervals, and the viral loads in the supernatants were determined by qRT-PCR to evaluate the effects of drugs on viral replication. Virus loads were expressed as the $\log_{10}$ number of copies per milliliter of cell supernatant.

To examine the treatments with type I, II, and III IFNs and ribavirin *in vivo*, three murine IFNs (IFN-α2a, IFN-γ, IFN-λ1), IL-1β, IL-6 (Multisciences Biotechnology Co., Ltd., Hangzhou, China), and the nucleoside analog ribavirin were selected on the basis of their antiviral activity *in vitro*. Five-day-old ICR mice (n = 10 per group) were i.m. challenged with lethal doses of WF057R (310 LD_{50}). Within 1 h of inoculation, each mouse was i.m. injected with different doses of cytokines (IFN-α2a, 666.75 U/mouse; IFN-γ, 833.25 U/mouse; IFN-λ1, 125 μg/mouse; IL-1β, 2,000 U/mouse; IL-6, 1,000 U/mouse; ribavirin 100 μg/mouse). The mortality rate and clinical symptoms were then monitored and recorded daily after infection until 12 days after inoculation.

Protective efficacy of anti-CVA6 serum and maternal antibodies. Prior to the evaluation of the protective efficacy of CVA6 antibodies, the neutralization titers of anti-CVA6 serum were determined by microneutralization assay. A previously described microneutralization assay was used to measure the antibody responses to EVA71, CVA16, and CVA6 (68). RD cells were used to seed 96-well plates at a density of 5×10^3 cells/well. When the plates were 90% confluent, individual serum samples were heat inactivated at 56°C for 30 min. Twofold serial dilutions of serum samples were mixed with equal volumes of viral suspensions (2,000 $TCID_{50}$/ml) and then incubated at 37°C for 1.5 h. A 100-μl volume of each serum-virus mixture was added to three wells (final virus titer, 310 $TCID_{50}$/well). Each well was scored for a CPE at 5 dpi. The endpoint neutralizing titer was defined as the highest serum dilution at which at least two of the three replicates were negative for a CPE.

To examine the protective role of the humoral immune response, two experiments were carried out. First, 5-day-old ICR mice (n = 10 per group) were i.m. inoculated with 310 LD_{50} of WF057R. Within 1 h of inoculation, each mouse was i.m. inoculated with 50 μl of 10-fold serially diluted mouse anti-CVA6 serum (10- to 10,000-fold dilutions) or negative serum. The mortality rate and clinical symptoms were then monitored and recorded daily for 12 days after inoculation with CVA6. The 50% protective dose obtained by a passive immunization protection test (ED_{50}I) was calculated with the Reed and Muench formula.

In the second experiment, the protective efficacy of maternal antibodies was studied. WF057R (9.6×10^5 $TCID_{50}$/ml) was inactivated by adding 37% formaldehyde (Sinopharm Group, Beijing, China) to viral suspensions to a final dilution of 1/4,000. The viral suspension was then incubated at 37°C for 3 days (69). The inactivated suspensions were filtered as described above and stored at −80°C. Eight-week-old female ICR mice (n = 4 per group) were i.m. injected twice 2 weeks apart with 50 μl of formaldehyde-inactivated CVA6 or medium. The mice were allowed to mate 1 h after the first injection. After delivery (about 5 to 10 days after the boost), pups were i.m. challenged with lethal doses of WF057R (310 LD_{50}) and four other CVA6 genotype E2 strains, WH15066 (300 LD_{50}), DY003R (300 LD_{50}), DY005R (300 LD_{50}), and LW03R (300 LD_{50}) (see Fig. S1 in the supplemental material), on postnatal day 5. The body weights, clinical symptoms, and mortality rates of the challenged suckling mice were monitored as described above. Male mice were euthanized, and serum samples were collected and stored at −80°C until use.

Evaluation of therapeutic efficacy of antivirus serum. Five-day-old ICR mice were inoculated i.m. with a lethal dose (310 LD_{50}) of WF057R. Mice at early (grade 1 to 2) and later (grade >3) infection stages were selected and divided into six experimental groups (n = 10 per group). The mice in the early and late infection groups were i.v. injected with 50 μl of different dilutions (1-, 10-, and 50-fold) of mouse anti-CVA6 serum and negative serum, separately. The mortality rates and clinical symptoms were monitored and recorded daily until 12 days after injection with antiserum. The 50% therapeutic dose obtained by a passive immunization protection test (ED_{50}II) was calculated with the Reed and Muench formula.

Statistical analysis. All statistical analysis was performed with GraphPad Prism Version 5.0 (GraphPad 4 Software, San Diego, CA, USA). The frequencies of survival and death in treated versus control mice

were assessed with the Mantel-Cox log rank test. The results were expressed as mean values and standard deviations. Differences in mean tissue viral titers, serum cytokine concentrations, and $TCID_{50}$ were determined with a two-tailed Mann-Whitney U test or a Kruskal-Wallis test. LD_{50}, ED_{50}I, and ED_{50}II were calculated as described by Reed and Muench (65). A difference was considered significant when the *P* value upon two-tailed *t* testing was <0.05.

Accession number(s). The genome sequences of the clinical isolates characterized in the present study, WF057R/CVA6/Shandong/China/2014, DY003R/CVA6/Shandong/China/2013, DY005R/CVA6/Shandong/China/2013, LW03R/CVA6/Shandong/China/2014, WH15066/CVA6/Shandong/China/2015, SD004R/EVA71/Shandong/China/2015, and LW30H/CVB4/Shandong/China/2015, have been deposited in GenBank under accession numbers KX752785, KY126089, KY126090, KY126091, KY126092, KY315729, and KX752784.

SUPPLEMENTAL MATERIAL

Supplemental material for this article may be found at https://doi.org/10.1128/JVI.02450-16.

SUPPLEMENTAL FILE 1, PDF file, 0.2 MB.

ACKNOWLEDGMENTS

We acknowledge the Shandong Provincial Center for Disease Control and Prevention for providing RD and Hep-2 cells.

This study was supported by grants from the Natural Science Foundation of Shandong Province (nos. ZR2014HP068 and ZR2015JL026) and the National Natural Science Foundation of China (no. 81601773). W.S. was supported by the Taishan Scholar Project of Shandong Province.

REFERENCES

1. Knowles NJ, Hovi T, Hyypia T, King AMQ, Lindberg AM, Pallansch MA, Palmenberg AC, Simmonds P, Skern T, Stanway G, Yamashita T, Zell R. 2011. Picornaviridae, p 855–880. *In* King AMQ, Adams MJ, Carstens EB, Lelkowitz EJ (ed), Virus taxonomy ninth report of the International Committee on Taxonomy of Viruses. Elsevier/Academic Press, London, United Kingdom.
2. Oberste MS, Maher K, Nix WA, Michele SM, Uddin M, Schnurr D, al-Busaidy S, Akoua-Koffi C, Pallansch MA. 2007. Molecular identification of 13 new enterovirus types, EV79-88, EV97, and EV100-101, members of the species human enterovirus B. Virus Res 128:34–42. https://doi.org/10.1016/j.virusres.2007.04.001.
3. Oberste MS, Maher K, Pallansch MA. 2004. Evidence for frequent recombination within species human enterovirus B based on complete genomic sequences of all thirty-seven serotypes. J Virol 78:855–867. https://doi.org/10.1128/JVI.78.2.855-867.2004.
4. Sun Q, Zhang Y, Zhu S, Tian H, Huang G, Cui H, Li X, Yan D, Zhu Z, Li J, Zheng P, Jiang H, Zhang B, Tan X, Zhu H, An H, Xu W. 2013. Transmission of human enterovirus 85 recombinants containing new unknown serotype HEV-B donor sequences in Xinjiang Uighur Autonomous Region, China. PLoS One 8:e55480. https://doi.org/10.1371/journal.pone.0055480.
5. Wang J, Zhang Y, Hong M, Li X, Zhu S, Yan D, Wang D, An H, Tsewang, Han J, Xu W. 2012. Isolation and characterization of a Chinese strain of human enterovirus 74 from a healthy child in the Tibet Autonomous Region of China. Arch Virol 157:1593–1598. https://doi.org/10.1007/s00705-012-1332-9.
6. Chen YJ, Chang SC, Tsao KC, Shih SR, Yang SL, Lin TY, Huang YC. 2012. Comparative genomic analysis of coxsackievirus A6 strains of different clinical disease entities. PLoS One 7:e52432. https://doi.org/10.1371/journal.pone.0052432.
7. Fujimoto T, Iizuka S, Enomoto M, Abe K, Yamashita K, Hanaoka N, Okabe N, Yoshida H, Yasui Y, Kobayashi M. 2012. Hand, foot, and mouth disease caused by coxsackievirus A6, Japan, 2011. Emerg Infect Dis 18:337–339. https://doi.org/10.3201/eid1802.111147.
8. Puenpa J, Chieochansin T, Linsuwanon P, Korkong S, Thongkomplew S, Vichaiwattana P, Theamboonlers A, Poovorawan Y. 2013. Hand, foot, and mouth disease caused by coxsackievirus A6, Thailand, 2012. Emerg Infect Dis 19:641–643. https://doi.org/10.3201/eid1904.121666.
9. Lim CT, Jiang L, Ma S, James L, Ang LW. 2016. Basic reproduction number of coxsackievirus type A6 and A16 and enterovirus 71: estimates from outbreaks of hand, foot and mouth disease in Singapore, a tropical city-state. Epidemiol Infect 144:1028–1034. https://doi.org/10.1017/S0950268815002137.
10. Kobayashi M, Makino T, Hanaoka N, Shimizu H, Enomoto M, Okabe N, Kanou K, Konagaya M, Oishi K, Fujimoto T. 2013. Clinical manifestations of coxsackievirus A6 infection associated with a major outbreak of hand, foot, and mouth disease in Japan. Jpn J Infect Dis 66:260–261. https://doi.org/10.7883/yoken.66.260.
11. Xing W, Liao Q, Viboud C, Zhang J, Sun J, Wu JT, Chang Z, Liu F, Fang VJ, Zheng Y, Cowling BJ, Varma JK, Farrar JJ, Leung GM, Yu H. 2014. Hand, foot, and mouth disease in China, 2008-12: an epidemiological study. Lancet Infect Dis 14:308–318. https://doi.org/10.1016/S1473-3099(13)70342-6.
12. Mirand A, Henquell C, Archimbaud C, Ughetto S, Antona D, Bailly JL, Peigue-Lafeuille H. 2012. Outbreak of hand, foot and mouth disease/herpangina associated with coxsackievirus A6 and A10 infections in 2010, France: a large citywide, prospective observational study. Clin Microbiol Infect 18:E110–E118. https://doi.org/10.1111/j.1469-0691.2012.03789.x.
13. Feder HM, Jr, Bennett N, Modlin JF. 2014. Atypical hand, foot, and mouth disease: a vesiculobullous eruption caused by Coxsackie virus A6. Lancet Infect Dis 14:83–86. https://doi.org/10.1016/S1473-3099(13)70264-0.
14. Banta J, Lenz B, Pawlak M, Laskoski K, Seykora C, Webber B, Yun H, Ritchie S. 2016. Notes from the field: outbreak of hand, foot, and mouth disease caused by coxsackievirus A6 among basic military trainees—Texas, 2015. MMWR Morb Mortal Wkly Rep 65:678–680. https://doi.org/10.15585/mmwr.mm6526a3.
15. Holmes CW, Koo SS, Osman H, Wilson S, Xerry J, Gallimore CI, Allen DJ, Tang JW. 2016. Predominance of enterovirus B and echovirus 30 as cause of viral meningitis in a UK population. J Clin Virol 81:90–93. https://doi.org/10.1016/j.jcv.2016.06.007.
16. Lu J, Zeng H, Zheng H, Yi L, Guo X, Liu L, Sun L, Tan X, Li H, Ke C, Lin J. 2014. Hand, foot and mouth disease in Guangdong, China, in 2013: new trends in the continuing epidemic. Clin Microbiol Infect 20:442–445. https://doi.org/10.1111/1469-0691.12468.
17. Li JL, Yuan J, Yang F, Wu ZQ, Hu YF, Xue Y, Zhou BP, Jin Q. 2014. Epidemic characteristics of hand, foot, and mouth disease in southern China, 2013. Coxsackievirus A6 has emerged as the predominant causative agent. J Infect 69:299–303. https://doi.org/10.1016/j.jinf.2014.04.001.
18. Di B, Zhang Y, Xie H, Li X, Chen C, Ding P, He P, Wang D, Geng J, Luo L, Bai Z, Yang Z, Wang M. 2014. Circulation of coxsackievirus A6 in hand-foot-mouth disease in Guangzhou, 2010–2012. Virol J 11:157–163. https://doi.org/10.1186/1743-422X-11-157.
19. Gao F, Mao QY, Chen P, Bian LL, Yao X, Li JX, Zhu FC, Liang ZL. 2016. Seroepidemiology of coxsackievirus A6, coxsackievirus A16, and entero-

virus 71 infections in infants and children: a prospective cohort study in Jiangsu, China. J Infect 73:509–512. https://doi.org/10.1016/j.jinf.2016.08.008.
20. Li J, Sun Y, Du Y, Yan Y, Huo D, Liu Y, Peng X, Yang Y, Liu F, Lin C, Liang Z, Jia L, Chen L, Wang Q, He Y. 2016. Characterization of coxsackievirus A6- and Enterovirus 71-Associated Hand Foot and Mouth Disease in Beijing, China, from 2013 to 2015. Front Microbiol 7:391. https://doi.org/10.3389/fmicb.2016.00391.
21. Du J, Wang X, Hu Y, Li Z, Li Y, Sun S, Yang F, Jin Q. 2014. Changing aetiology of hand, foot and mouth disease in Linyi, China, 2009–2011. Clin Microbiol Infect 20:O47–49. https://doi.org/10.1111/1469-0691.12301.
22. He YQ, Chen L, Xu WB, Yang H, Wang HZ, Zong WP, Xian HX, Chen HL, Yao XJ, Hu ZL, Luo M, Zhang HL, Ma HW, Cheng JQ, Feng QJ, Zhao DJ. 2013. Emergence, circulation, and spatiotemporal phylogenetic analysis of coxsackievirus A6- and coxsackievirus A10-associated hand, foot, and mouth disease infections from 2008 to 2012 in Shenzhen, China. J Clin Microbiol 51:3560–3566. https://doi.org/10.1128/JCM.01231-13.
23. Bian L, Wang Y, Yao X, Mao Q, Xu M, Liang Z. 2015. Coxsackievirus A6: a new emerging pathogen causing hand, foot and mouth disease outbreaks worldwide. Expert Rev Anti Infect Ther 13:1061–1071. https://doi.org/10.1586/14787210.2015.1058156.
24. Bracho MA, González-Candelas F, Valero A, Córdoba J, Salazar A. 2011. Enterovirus co-infections and onychomadesis after hand, foot, and mouth disease, Spain, 2008. Emerg Infect Dis 17:2223–2231. https://doi.org/10.3201/eid1712.110395.
25. Osterback R, Vuorinen T, Linna M, Susi P, Hyypiä T, Waris M. 2009. Coxsackievirus A6 and hand, foot, and mouth disease, Finland. Emerg Infect Dis 15:1485–1488. https://doi.org/10.3201/eid1509.090438.
26. Yasui Y, Makino T, Hanaoka N, Owa K, Horikoshi A, Tanaka A, Suehiro Y, Shimizu H, Kanou K, Kobayashi M, Konagaya M, Fujimoto T. 2013. A case of atypical hand-foot-and-mouth disease caused by coxsackievirus A6: differential diagnosis from varicella in a pediatric intensive care unit. Jpn J Infect Dis 66:564–566. https://doi.org/10.7883/yoken.66.564.
27. Downing C, Ramirez-Fort MK, Doan HQ, Benoist F, Oberste MS, Khan F, Tyring SK. 2014. Coxsackievirus A6 associated hand, foot and mouth disease in adults: clinical presentation and review of the literature. J Clin Virol 60:381–386. https://doi.org/10.1016/j.jcv.2014.04.023.
28. Guimbao J, Rodrigo P, Alberto MJ, Omeñaca M. 2010. Onychomadesis outbreak linked to hand, foot, and mouth disease, Spain, July 2008. Euro Surveill 15:1. http://www.eurosurveillance.org/ViewArticle.aspx?ArticleId=19663.
29. Wei SH, Huang YP, Liu MC, Tsou TP, Lin HC, Lin TL, Tsai CY, Chao YN, Chang LY, Hsu CM. 2011. An outbreak of coxsackievirus A6 hand, foot, and mouth disease associated with onychomadesis in Taiwan, 2010. BMC Infect Dis 11:346. https://doi.org/10.1186/1471-2334-11-346.
30. Rao CD, Yergolkar P, Shankarappa KS. 2012. Antigenic diversity of enteroviruses associated with nonpolio acute flaccid paralysis, India, 2007–2009. Emerg Infect Dis 18:1833–1840. https://doi.org/10.3201/eid1811.111457.
31. Blomqvist S, Klemola P, Kaijalainen S, Paananen A, Simonen ML, Vuorinen T, Roivainen M. 2010. Co-circulation of coxsackieviruses A6 and A10 in hand, foot and mouth disease outbreak in Finland. J Clin Virol 48:49–54. https://doi.org/10.1016/j.jcv.2010.02.002.
32. Logotheti M, Pogka V, Horefti E, Papadakos K, Giannaki M, Pangalis A, Sgouras D, Mentis A. 2009. Laboratory investigation and phylogenetic analysis of enteroviruses involved in an aseptic meningitis outbreak in Greece during the summer of 2007. J Clin Virol 46:270–274. https://doi.org/10.1016/j.jcv.2009.07.019.
33. Richter J, Koptides D, Tryfonos C, Christodoulou C. 2006. Molecular typing of enteroviruses associated with viral meningitis in Cyprus, 2000–2002. J Med Microbiol 55(Pt 8):1035–1041. https://doi.org/10.1099/jmm.0.46447-0.
34. Jiang FC, Hao B, Dong LY. 2013. Etiological analysis of hand, foot and mouth disease in Qingdao, 2007–2011. Chin J Dis Control Prev 17:153–155. (in Chinese.)
35. Kirkwood J. 2002. Cancer immunotherapy: the interferon-alpha experience. Semin Oncol 29(3 Suppl 7):18–26. https://doi.org/10.1053/sonc.2002.33078.
36. Yang J, Yang C, Guo N, Zhu K, Luo K, Zhang N, Zhao H, Cui Y, Chen L, Wang H, Gu J, Ge B, Qin CF, Leng Q. 2015. Type I interferons triggered through the TLR3-TRIF pathway control coxsackievirus A16 infection in young mice. J Virol 89:10860–10867. https://doi.org/10.1128/JVI.01627-15.
37. Liu ML, Lee YP, Wang YF, Lei HY, Liu CC, Wang SM, Su IJ, Wang JR, Yeh TM, Chen SH, Yu CK. 2005. Type I interferons protect mice against enterovirus 71 infection. J Gen Virol 86(Pt 12):3263–3269. https://doi.org/10.1099/vir.0.81195-0.
38. Liu CC, Chow YH, Chong P, Klein M. 2014. Prospect and challenges for the development of multivalent vaccines against hand, foot and mouth diseases. Vaccine 32:6177–6182. https://doi.org/10.1016/j.vaccine.2014.08.064.
39. Bek EJ, Hussain KM, Phuektes P, Kok CC, Gao Q, Cai F, Gao Z, McMinn PC. 2011. Formalin-inactivated vaccine provokes cross-protective immunity in a mouse model of human enterovirus 71 infection. Vaccine 29:4829–4838. https://doi.org/10.1016/j.vaccine.2011.04.070.
40. Ong KC, Devi S, Cardosa MJ, Wong KT. 2010. Formaldehyde-inactivated whole-virus vaccine protects a murine model of enterovirus 71 encephalomyelitis against disease. J Virol 84:661–665. https://doi.org/10.1128/JVI.00999-09.
41. Mao Q, Wang Y, Gao R, Shao J, Yao X, Lang S, Wang C, Mao P, Liang Z, Wang J. 2012. A neonatal mouse model of coxsackievirus A16 for vaccine evaluation. J Virol 86:11967–11976. https://doi.org/10.1128/JVI.00902-12.
42. Liu Q, Shi J, Huang X, Liu F, Cai Y, Lan K, Huang Z. 2014. A murine model of coxsackievirus A16 infection for anti-viral evaluation. Antiviral Res 105:26–31. https://doi.org/10.1016/j.antiviral.2014.02.015.
43. Dong C, Wang J, Liu L, Zhao H, Shi H, Zhang Y, Jiang L, Li Q. 2010. Optimized development of a candidate strain of inactivated EV71 vaccine and analysis of its immunogenicity in rhesus monkeys. Hum Vaccine 6:1028–1037. https://doi.org/10.4161/hv.6.12.12982.
44. Yang L, Mao Q, Li S, Gao F, Zhao H, Liu Y, Wan J, Ye X, Xia N, Cheng T, Liang Z. 2016. A neonatal mouse model for the evaluation of antibodies and vaccines against coxsackievirus A6. Antiviral Res 134:50–57. https://doi.org/10.1016/j.antiviral.2016.08.025.
45. Yang L, Li S, Liu Y, Hou W, Lin Q, Zhao H, Xu L, He D, Ye X, Zhu H, Cheng T, Xia N. 2015. Construction and characterization of an infectious clone of coxsackievirus A6 that showed high virulence in neonatal mice. Virus Res 210:165–168. https://doi.org/10.1016/j.virusres.2015.08.002.
46. Deng H, Zhang Y, Ma C, Fu J, Zhang Y, Xie Y, Yuan J, Wang X. 2015. Pathogenic and clinical presentation of bullous rash in hand, foot and mouth disease. Zhonghua Er Ke Za Zhi 53:616–620. (in Chinese.)
47. Khong WX, Foo DG, Trasti SL, Tan EL, Alonso S. 2011. Sustained high levels of interleukin-6 contribute to the pathogenesis of enterovirus 71 in a neonate mouse model. J Virol 85:3067–3076. https://doi.org/10.1128/JVI.01779-10.
48. Yu P, Gao Z, Zong Y, Bao L, Xu L, Deng W, Li F, Lv Q, Gao Z, Xu Y, Yao Y, Qin C. 2014. Histopathological features and distribution of EV71 antigens and SCARB2 in human fatal cases and a mouse model of enterovirus 71 infection. Virus Res 189:121–132. https://doi.org/10.1016/j.virusres.2014.05.006.
49. Lin YW, Yu SL, Shao HY, Lin HY, Liu CC, Hsiao KN, Chitra E, Tsou YL, Chang HW, Sia C, Chong P, Chow YH. 2013. Human SCARB2 transgenic mice as an infectious animal model for enterovirus 71. PLoS One 8:e57591. https://doi.org/10.1371/journal.pone.0057591.
50. Koyuncu OO, Hogue IB, Enquist LW. 2013. Virus infections in the nervous system. Cell Host Microbe 13:379–393. https://doi.org/10.1016/j.chom.2013.03.010.
51. Ong KC, Badmanathan M, Devi S, Leong KL, Cardosa MJ, Wong KT. 2008. Pathologic characterization of a murine model of human enterovirus 71 encephalomyelitis. J Neuropathol Exp Neurol 67:532–542. https://doi.org/10.1097/NEN.0b013e31817713e7.
52. Clark RS, Carlos TM, Schiding JK, Bree M, Fireman LA, DeKosky ST, Kochanek PM. 1996. Antibodies against Mac-1 attenuate neutrophil accumulation after traumatic brain injury in rats. J Neurotrauma 13:333–341.
53. Lin TY, Hsia SH, Huang YC, Wu CT, Chang LY. 2003. Proinflammatory cytokine reactions in enterovirus 71 infections of the central nervous system. Clin Infect Dis 36:269–274. https://doi.org/10.1086/345905.
54. Ye N, Gong X, Pang LL, Gao WJ, Zhang YT, Li XL, Liu N, Li DD, Jin Y, Duan ZJ. 2015. Cytokine responses and correlations thereof with clinical profiles in children with enterovirus 71 infections. BMC Infect Dis 15:225. https://doi.org/10.1186/s12879-015-0965-1.
55. Chen Z, Li R, Xie Z, Huang G, Yuan Q, Zeng J. 2014. IL-6, IL-10 and IL-13 are associated with pathogenesis in children with enterovirus 71 infection. Int J Clin Exp Med 7:2718–2723.
56. Wang SM, Lei HY, Su LY, Wu JM, Yu CK, Wang JR, Liu CC. 2007. Cerebrospinal fluid and cytokines in enterovirus 71 brain stem en-

cephalitis and echovirus meningitis infections of varying severity. Clin Microbiol Infect 13:677–682. https://doi.org/10.1111/j.1469-0691.2007.01729.x.
57. Wang SM, Lei HY, Huang KJ, Wu JM, Wang JR, Yu CK, Su IJ, Liu CC. 2003. Pathogenesis of enterovirus 71 brainstem encephalitis in pediatric patients: roles of cytokines and cellular immune activation in patients with pulmonary edema. J Infect Dis 188:564–570. https://doi.org/10.1086/376998.
58. Lin TY, Chang LY, Hsia SH, Huang YC, Chiu CH, Hsueh C, Shih SR, Liu CC, Wu MH. 2002. The 1998 enterovirus 71 outbreak in Taiwan: pathogenesis and management. Clin Infect Dis 34:S52–S57. https://doi.org/10.1086/338819.
59. Kosai K, Seki M, Yanagihara K, Nakamura S, Kurihara S, Izumikawa K, Kakeya H, Yamamoto Y, Tashiro T, Kohno S. 2008. Gabexate mesilate suppresses influenza pneumonia in mice through inhibition of cytokines. J Int Med Res 36:322–328. https://doi.org/10.1177/147323000803600215.
60. Wang SM, Lei HY, Huang MC, Su LY, Lin HC, Yu CK, Wang JL, Liu CC. 2006. Modulation of cytokine production by intravenous immunoglobulin in patients with enterovirus 71-associated brainstem encephalitis. J Clin Virol 37:47–52. https://doi.org/10.1016/j.jcv.2006.05.009.
61. Wang SM, Liu CC. 2009. Enterovirus 71: epidemiology, pathogenesis and management. Expert Rev Anti Infect Ther 7:735–742. https://doi.org/10.1586/eri.09.45.
62. Nolan MA, Craig ME, Lahra MM, Rawlinson WD, Prager PC, Williams GD, Bye AM, Andrews PI. 2003. Survival after pulmonary edema due to enterovirus 71 encephalitis. Neurology 60:1651–1656. https://doi.org/10.1212/01.WNL.0000066810.62490.FF.
63. Arya SC. 2000. Antiviral therapy for neurological manifestations of enterovirus 71 infection. Clin Infect Dis 30:988–992. https://doi.org/10.1086/313837.
64. McConnell J. 1999. Enteroviruses succumb to new drug. Lancet 354:1185.
65. Reed LJ, Muench H. 1938. A simple method of estimating 50 percent end-points. Am J Epidemiol 27:493–497. https://doi.org/10.1093/oxfordjournals.aje.a118408.
66. Bubba L, Pellegrinelli L, Pariani E, Primache V, Amendola A, Binda S. 2015. A novel multiplex one-step real-time RT-PCR assay for the simultaneous identification of enterovirus and parechovirus in clinical fecal samples. J Prev Med Hyg 56:E57–E60.
67. Liu F, Liu Q, Cai Y, Leng Q, Huang Z. 2011. Construction and characterization of an infectious clone of coxsackievirus A16. Virol J 8:534. https://doi.org/10.1186/1743-422X-8-534.
68. Caine EA, Fuchs J, Das SC, Partidos CD, Osorio JE. 2015. Efficacy of a trivalent hand, foot, and mouth disease vaccine against enterovirus 71 and coxsackieviruses A16 and A6 in mice. Viruses 7:5919–5932. https://doi.org/10.3390/v7112916.
69. Martín J, Crossland G, Wood DJ, Minor PD. 2003. Characterization of formaldehyde-inactivated poliovirus preparations made from live attenuated strains. J Gen Virol 84:1781–1788. https://doi.org/10.1099/vir.0.19088-0.